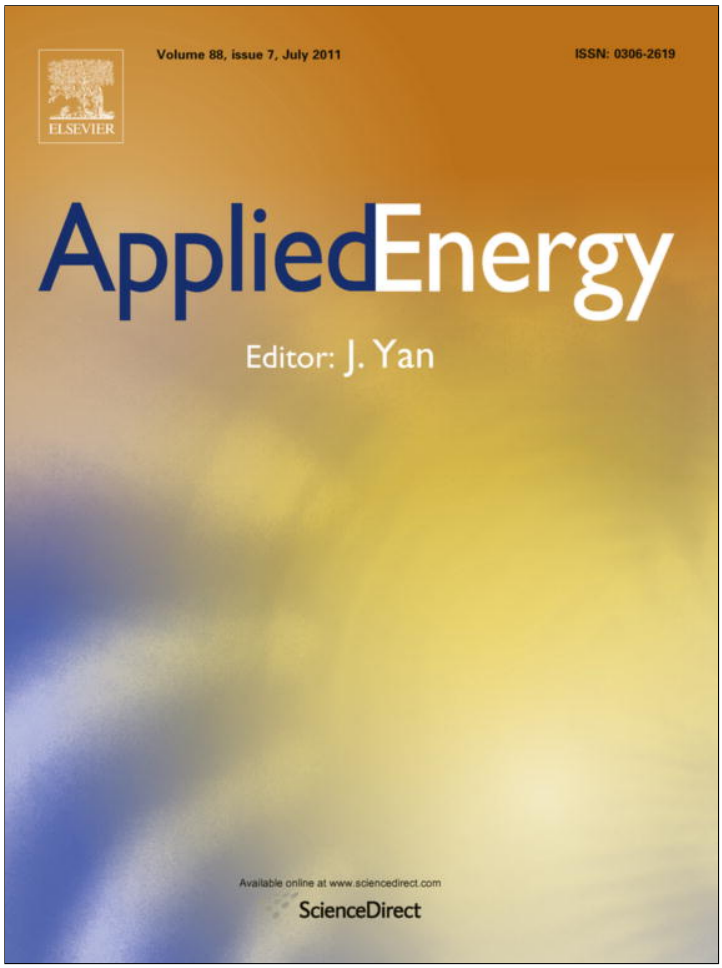

Applied Energy 88 (2011) 2454–2462

Contents lists available at ScienceDirect

Applied Energy

journal homepage: www.elsevier.com/locate/apenergy

Experimental and numerical investigation of a phase change material: Thermal-energy storage and release

Annabelle Joulin [a,b,*], Zohir Younsi [c], Laurent Zalewski [a,b], Stéphane Lassue [a,b], Daniel R. Rousse [d], Jean-Paul Cavrot [e]

[a] Univ Lille Nord de France, F59000 Lille, France
[b] UArtois, LGCgE, F-62400 Béthune Cedex, France
[c] HEI, rue de Toul, 59000 Lille, France
[d] Department of Applied Sciences – Université du Québec à Chicoutimi, 555, boulevard de l'Université, Chicoutimi QC, Canada G7H 2B1
[e] UCCS Artois, IUT de Béthune, BP819, 62408 Béthune Cedex, France

ARTICLE INFO

Article history:
Received 14 June 2010
Received in revised form 7 January 2011
Accepted 13 January 2011

Keywords:
Phase change material
Energy storage
Supercooling
Enthalpy method
Fluxmetric experiments

ABSTRACT

The application of phase change materials (PCMs) for solar thermal-energy storage capacities has received considerable attention in recent years due to their large storage capacity and isothermal nature of the storage process. This study deals with the comparison of numerical and experimental results for a PCM conditioned in a parallelepipedic polyefin envelope to be used in passive solar walls. The experimental results were obtained by use of a genuine set-up involving heat flux sensors and thermocouples mounted on two vertical aluminium exchanger plates squeezing the samples. Numerical predictions were obtained with a custom one-dimensional Fortran code and a two-dimensional use of Fluent. Both methods showed a very good agreement with experimental observations for the melting process ($\leqslant$5%). However during solidification, both numerical codes failed to predict the phase change process accurately, the maximal relative error was as high as 57% (with an average of 8%).

1. Introduction

An extensive amount of research of problems involving phase change solid–liquid (fusion or solidification) has been done in various scientific and technological domains as well as for industrial applications [1], such as, metallurgy and petrochemical industries, glass and plastic companies, food industries, thermal control of spacecrafts, heat exchanger [2], water purification [3] and so on. These systems are used in order to store thermal energy for a period while the supply is sufficient or cheaper, to be discharged when the supply becomes insufficient or expensive [4,5]. The high thermal storage capacity of a phase change material (PCM) can reduce energy consumption in buildings [6,7]. PCM can be used to absorb heat gains during daytime and release heat at night.

They could also be used for cooling and ventilation application to reduce energy consumption in buildings during summer period [8,9]. Thermal-energy storage can be accomplished either by using sensible heat storage or latent heat storage. Sensible heat storage has been used for centuries by builders to store/release passive thermal energy. In general, a much larger volume of material is required to store the same amount of energy in comparison to latent heat storage [4,10,11]. The principle of the use of phase change materials (PCMs) is simple. As the temperature increases, the material changes phase from solid to liquid. Because the reaction is endothermic, the PCM absorbs heat. Similarly, when the temperature decreases, the material changes phase from liquid to solid, and the PCM releases heat [2].

Zalba et al. [12] carried out of the history review of thermal-energy storage with solid–liquid phase change materials in materials selection, heat transfer and applications. A great number of organic, inorganic, polymeric and eutectic compounds have been used as phase change materials, such as polyethylene glycol (PEG) and their composites (PEG/SiO2 [13] and so on). In order to improve the thermal conductivity of these PCMs, Wang et al. [14,15] added b-Aluminium nitride and expanded graphite into the organic PCMs. Salt hydrates are popular phase change materials (PCMs) for thermal-energy storage because of their high value of latent heat. Many of these substances are prone to supercooling, which for normal applications is problematic as it prevents the release of the stored latent heat.

In the present paper, a detailed study on the thermal storage capacity of a phase change material for energy conservation in buildings, and in particular in solar walls, is analyzed and discussed.

* Corresponding author at: Univ Lille Nord de France, F59000 Lille, France. Tel.: +33 321632356; fax: +33 321632366.
E-mail address: annabelle.joulin@univ-artois.fr (A. Joulin).

0306-2619/$ - see front matter © 2011 Elsevier Ltd. All rights reserved.
doi:10.1016/j.apenergy.2011.01.036

Nomenclature

c_p	specific heat (J/kg °C)
e	width of the brick
f	liquid fraction
h	sensible volumetric enthalpy (J/m^3)
k	thermal conductivity (W/mK)
t	time (s)
T	temperature (°C)
x	space coordinate (m)
α	thermal diffusivity (m^2/s)
ρ	density (kg/m^3)
μ	dynamic viscosity (Pa s)
ϕ	heat flux (W/m^2)
L_x	horizontal domain length (m)
L_y	vertical domain length (m)
L_f	latent heat of fusion (J/kg)
R	aspect ratio

Subscripts

0	initial temperature
E	east node
F	final temperature
P	center node
W	west node
k	relative to phase k

Superscripts

k	iteration level
l	liquid phase
o	old value
s	solid phase

Non-dimensional numbers

Pr	Prandtl number
Ra	Rayleigh number
Ste	Stefan number

As the overall objective is to insert PCMs in a passive solar component such as the «composite Trombe wall», parametric studies of relevant properties and dimensions are required. For example, the target climate for the use of PCM 27 in Trombe solar walls is a temperate climate with usual ambient temperatures. The temperature of the material cannot exceed 60 °C, because the PCM may lose its storage capacity and it could be damaged (phenomenon of segregation).

Concerning the implementation, it is very interesting to envisage important heat storage within PCMs in a relative small volume. In the case of solar energy channeled, it is important because the heat flux can be intense during a short period. Experimental and numerical works confirm the difficulty to control the solidification process often accompanied of the unpredictable supercooling phenomenon dependant of the heat transfer dynamics. It also has an influence on the heat recovery evolving on larger periods, the heat fluxes are smaller. In the context of our application, the restitution of the heat stored can be done in natural convection or eventually in forced convection by means of a fan. This involves obtaining the best heat transfer conditions to store energy in a reasonable time interval. It has to be examined in a future work.

An experimental set-up consisting of fluxmetric measurement has been constructed to provide the thermal performance of the PCM. In addition, a DSC analysis was carried out. Moreover, a mathematical model has been developed. A Fortran code 1D and the commercial CFD software Fluent were applied for the computation of the thermal behaviour of the PCM. A comparison with the experimental results was made and several simulation runs were conducted to provide the heat storage during the melting process.

2. Material characterization

The studied material (hydrated salts, mineral, containing potassium and calcium chlorides) has a melting point provided by the manufacturer equal to +27 °C [16]. Its thermophysical properties are summarized in Table 1.

Generally, these materials are characterized by calorimetric experiments like Differential Scanning Calorimetry (DSC) and differential thermal analysis (DTA) [17–20], which are applied to very small quantities of products. In this study, the melting temperature and fusion heat of the PCM were measured by a DSC instrument (Perkin–Elmer Pyris calorimeter). All DSC measurements were repeated for each sample at a different heating rate to ensure the reproducibility. Finally, a 5 °C/min heating rate was employed and considered sufficient for the experiments in the case of fusion.

Samples were conditioned in aluminium pans [21]. The DSC thermal analyses were performed in the temperature range of −30 °C/+50 °C. The melting temperature of the PCM corresponds to the onset temperature (31.74 °C) obtained by the conventional procedure as the intersecting point between the tangent line at the point of the maximum slope of the DSC peak and the non linear base line taking into account the change of heat capacity between the solid and the liquid phases (Fig. 1) [22]. The result is relatively inconsistent with the value provided by the product manufacturer (+26.9 °C). The latent heat of fusion was calculated as the area under the peak by numerical integration (L_f = 186.6 kJ/kg) [23].These values are taken as representative of the thermal behaviour of the material as the exact quantitative composition of the salts mixture and the corresponding phase diagram are unknown.

In case of cooling, problems were even more complex. With our material (PCM 27), solidification process analysis has been impossible because of the importance of the supercooling phenomenon in the PCM. Experiments undertaken with different sample weights and different temperature cycles led to crystallization temperatures between −2 °C and 10 °C with no reproducibility. The supercooling phenomenon is particularly important in DSC measurements as they use small samples in a well thermally isolated cell. The phenomenon of supercooling may be an obstacle in industrial processes if its effect becomes significant.

To overcome this problem and to clarify the effects on the heat transfer performance, a second experimental device was developed, based on the measurement of temperatures and heat fluxes exchanged between the two lateral sides of the PCM samples, providing the total heat stored during the phase change process.

Table 1
Thermophysical properties of PCM 27.

Variable	PCM 27	
	Solid	Liquid
k (W/m K)	0.577	0.813
c_p (J/kg K)	1751.5	2225
α (m^2/s)	1.93×10^{-7}	2.39×10^{-7}
ρ (kg/m^3)	1710	1530
L_f (kJ/kg)	172.42	
μ (Pa s)		0.094

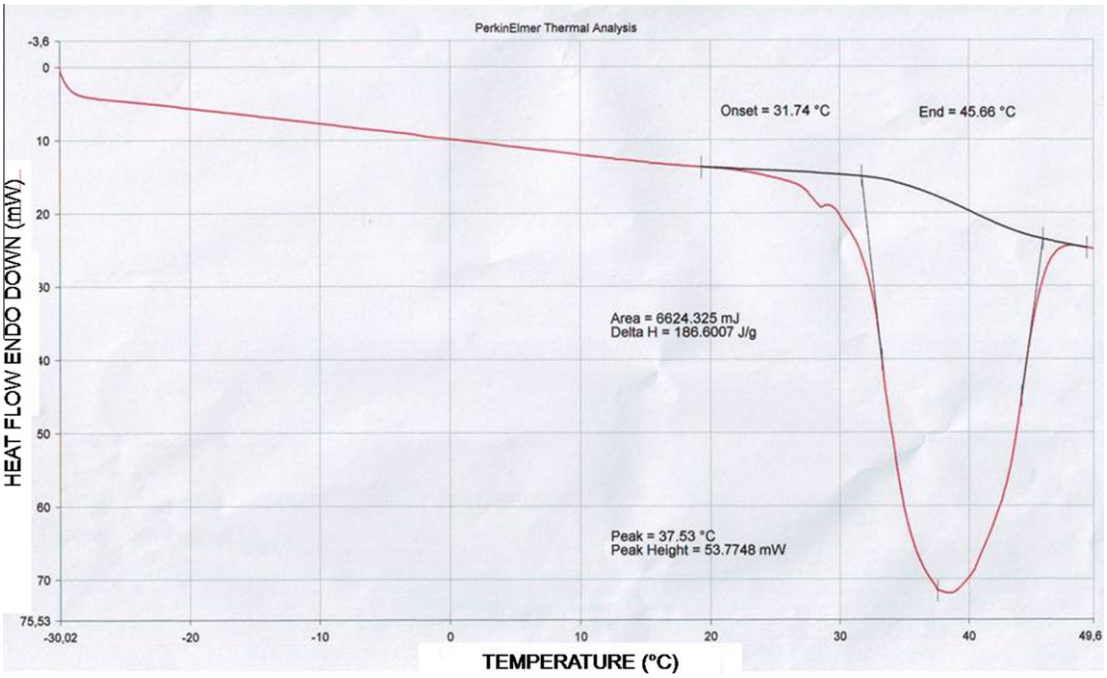

Fig. 1. Differential scanning calorimetry application (5 °C/min).

3. Physical and mathematical models

The problem to be considered was that of a rectangular brick that initially held a solid PCM at temperature (T_0), lower than the melting temperature (T_F). This temperature was maintained until thermal equilibrium. The whole material was entirely solid. At time $t > 0$, the temperature of the outer left surface of the brick was increased to a constant temperature (T_W), such that $T_W > T_F$ (fusion process). Heat was conducted through the wall of the PCM brick, causing the PCM to start to melt next to the inner surface. The details of the experimental set-up and the mathematical model that were used to predict this melting process are outlined next.

3.1. Experimental set-up

Detailed discussion of the experimental set-up is provided elsewhere [24]. A schematic drawing of the PCM brick and its set-up are given in Fig. 2. The PCM was held in bricks of dimensions ($210 \times 140 \times 25$ mm^3). It was conditioned in a rectangular envelope and laid out vertically. The sample was placed between two heat exchanger plates of aluminium ($500 \times 500 \times 19$ mm^3). The lateral side faces were insulated by a 10 cm thick polyurethane foam which created a ring isolating the sample and minimized the heat transfer to the external ambient conditions.

The experimental set-up allowed to measure temperature fluctuations and heat flux exchanged during fusion and solidification processes. A temperature could be set on both sides of the PCM brick by means of a thermo regulated bath. These baths (Polystat CC3) allowed a fine regulation of the injected water temperature with a precision of 0.1 °C, and were connected to a cooling tank with a capacity of 25 l. The temperature range of this reservoir was between −30 °C and +200 °C. In this work, the temperature was varied between +15 °C and +50 °C.

Thermocouples T-type of sensitivity ($K = 40$ μV/°C) were placed outside the PCM brick. Between the exchanging plates and the

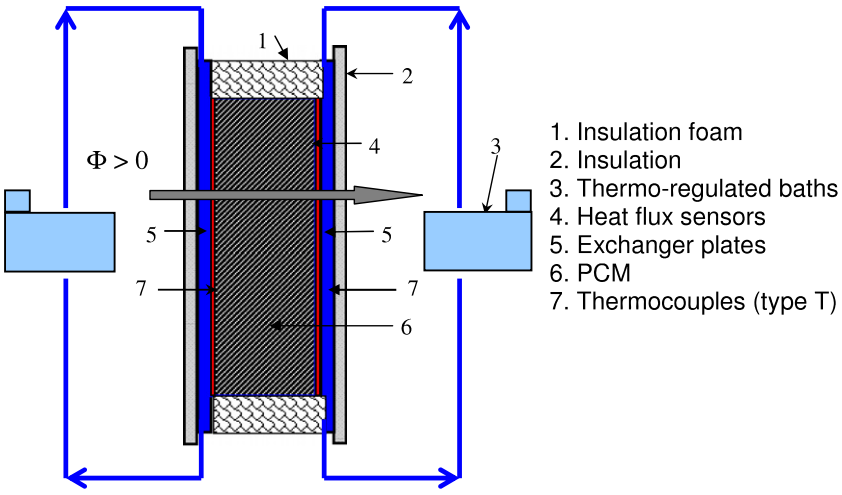

Fig. 2. Experimental device.

sample, heat flux sensors and thermocouples (T) (diameter 0.1 mm) were inserted in the envelope of the brick. The whole system was maintained vertical using a pneumatic jack. The fluxmeters used here were special ones called "with tangential gradients" [25]. Their thickness was about 0.2 mm, their dimensions were those of the brick (210 × 140 mm), and their sensitivity was about 110 μV/(W/m^2). These sensors were developed by our laboratory several years ago and were the subject of regular developments making possible to obtain a highly reliable measuring instrument. These fluxmeters were calibrated in house, using plane electrical resistances with sizes rigorously equal to those of the sensors. The calibration device described by [26] permitted to calibrate these sensors with a precision about ±3% of the full scale. The temperature measurements were differentials compared to a reference sensor placed in the heart of a thermal sink very stable in temperature. The various sensors were connected to a multichannel multimeter "Keithley 2700" adapted to low level signals measurement. Experimental data were recorded with regular and adjustable time steps.

3.2. Governing equations

A combined experimental/computational study was undertaken. Simulations were carried out first using a 1D finite difference code (FDM), and second, using a commercial software Fluent (2D simulations). This section presents the description of these codes. In association with the requirement for the PCM, the pertinent assumptions are:

1. The problem is one-dimensional (FDM code) and two-dimensional (Fluent).
2. Radiative heat transfer is neglected.
3. Thermophysical properties are constant. Although different in the liquid and the solid phases, densities, heat capacities, and thermal conductivities are assumed to remain constant with time and to be independent of temperature. Properties for PCM 27 were determined experimentally.
4. The PCM material is pure, homogeneous, and isotropic. This is certainly not the case for a hydrated salt as shown in Fig. 3 for the crystallization of PCM 27. Two types of crystallization are shown in Fig. 3. One can distinguish heterogeneous nuclei, which are not only linked to the fluid nature, but to the thermal effects, appearing on the lateral walls of the PCM brick, from the homogeneous nuclei, appearing in a chaotic manner in the center of the brick, and directly linked to the fluid nature. This picture represents a polycrystallized material.

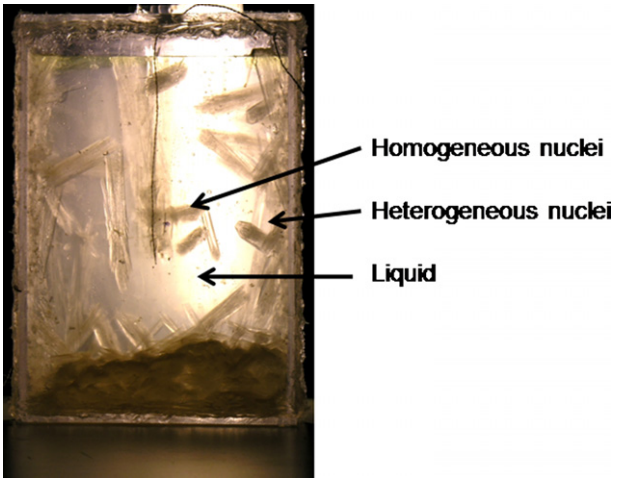

Fig. 3. Solidification process, visualization of heterogeneous crystallization.

To experimentally determine solid and liquid thermal apparent conductivities of the PCM inside the brick, a temperature difference was imposed between the two lateral sides of the PCM brick until observing a zero heat flux (equilibrium state).

$$k_{S,l} = \frac{e \cdot \sum \phi_{S,l}}{2 \cdot \Delta T_{S,l}} \tag{1}$$

where e is the dimension of the material, $\sum \varphi_{S,l}$ is the sum of the measured heat fluxes. Several tests were carried out on the material to check the reproducibility of the measurement. The results were found to be satisfactory and provided median values of apparent thermal conductivities: 0.600 W/m °C for the liquid and of 0.450 W/m °C for the solid. The estimated error on conductivity measurements is about 8%.

3.2.1. FDM code

The enthalpy formulation of the governing equation was used, since it represents the whole energy per unit mass in the studied domain. The heat transfer linked to the phase change was isolated via a source term present in the energy equation or an apparent specific heat [27]. The total amount of energy stored can be obtained from:

$$Q = \int_{Ti}^{Tf} \Delta\phi dt \tag{2}$$

where $\Delta\varphi$ represent the cumulative heat rate entering the sample through the thermo regulated plates. This cumulative quantity can also be expressed by:

$$Q = c_{PS}\Delta T_S + L_f + c_{Pl}\Delta T_l \tag{3}$$

where c_{pS} and c_{Pl} are the average solid state and the liquid state specific heats of the material, ΔT_s and ΔT_l are the temperature variations for the material in solid phase and in liquid phase, and L_f is the latent heat of fusion.

The prediction of stored heat according to Eq. (3) was validated by comparing the quantity of stored energy measured experimentally using the fluxmeters (by numerical integration of heat fluxes from 15 °C to 50 °C). The difference between measured (283.366 kJ) and calculated (280.807 kJ) values was less than 1% for the test brick (1.240 kg).

Thus, the governing partial differential equation for the phase change process can be written as:

$$\frac{\partial h}{\partial t} = \alpha \frac{\partial^2 h}{\partial x^2} - \rho L_f \frac{\partial f}{\partial t} \tag{4}$$

where

$$h = \int_{T_F}^{T} \rho c_p dT$$

and

$$\alpha = \frac{k}{\rho c_P} \tag{5}$$

The liquid fraction (f) is given by:

$$f = \begin{cases} 0 & \text{if } T < T_F \quad (solid) \\ 0-1 & \text{if } T = T_F \quad (mushy) \\ 1 & \text{if } T > T_F \quad (liquid) \end{cases} \tag{6}$$

3.2.1.1. Numerical solution 1D. Eq. (4) can be solved using a fully implicit finite difference solution method. The discretization of this equation leads to the scheme:

$$h_P = h_P^0 + \alpha R(h_E + h_W - 2h_P) + \rho L_f(f_P^0 - f_P^k) \tag{7}$$

$$a_P h_P + a_E h_E + a_W h_W = Q$$

where

$$\begin{aligned} a_P &= 1 + 2\alpha R \\ a_E &= a_W = -\alpha R \\ Q &= h_P^0 + \rho L_f (f_P^0 - f_P^k) \\ R &= \frac{\Delta t}{(\Delta x)^2} \end{aligned} \tag{8}$$

Here, h_P^0 and f_P^0 represent the enthalpy and the liquid fractions from the previous time step. Source term Q keeps track of the heat evolution and superscript k means the kth iteration of f at node P.

Eq. (7) has been solved using a tri-diagonal matrix algorithm (TDMA) and the liquid fraction update method [28]. When the phase change was occurring ($0 < f < 1$), the $(k+1)$th estimate of the melt fraction needed to be updated such that $h_P = 0$ in Eq. (7)

$$f_P^{k+1} = \frac{-a_E h_E - a_W h_W + h_P^0}{\rho L} + f_P^0 \tag{9}$$

Eq. (9) was applied at each node along with under/over correction:

$$f = \begin{cases} 0 & \text{if } f_P^{k+1} \leqslant 0 \\ 1 & \text{if } f_P^{k+1} \geqslant 1 \end{cases} \tag{10}$$

Convergence at a given time step was obtained when the difference between the total enthalpy fields was below than a given tolerance (10^{-4}).

$$\frac{ABS(H^k - H^{k+1})}{\rho_k c_k} \leqslant 10^{-4} \tag{11}$$

The boundary conditions were:

$$At \begin{vmatrix} t = 0 & 0 \leqslant x \leqslant L_x & T = T_0 < T_F \\ t > 0 & x = 0 & T = T_W > T_F \\ t < 0 & x = L_x & T = T_0 < T_F \end{vmatrix} \tag{12}$$

3.2.1.2. Algorithm. Different steps were required to solve algebraic equations [29–31]:

1. Solve Eq. (7) (TDMA algorithm);
2. update the liquid fraction at every nodes;
3. apply the correction (10);
4. check convergence criterion (11);
5. if the convergence criterion is not satisfied, go back at step 1.

Several simulations have been done in order to check the stability of the obtained solution. It was influenced by three different factors, namely the time step, the under-relaxation factor and the grid size (number of nodes).

3.2.1.3. Validation. The validation of the FDM code was performed in 1D and in 2D and the results were presented in another paper [32].

Numerical results (FDM) in 1D were compared with the analytical DIRICHLET for three different materials, namely ice, gallium and PCM 27 [32]. For example, the relative error is given in Table 2 for the fusion of ice. This study concerned with a semi-infinite problem whereas the numerical solution was obtained for a finite domain, sufficiently long to avoid sharp changes in temperature. Thermophysical properties and parameters are given in Tables 3–5 for these materials. For all the numerical tests, the length of the domain was 1 m. Several time steps have been studied. Initially at $t = 0$, the ice was at the uniform temperature $T_0 = 268.15$ K. At $t > 0$ and at $x = 0$, the temperature of the PCM was raised to $T_w = 293.15$ K, and the ice melting started, whereas the temperature at $x = L_x$ was maintained at $T_0 = 268.15$ K. The position of the interface has been studied for three different time steps (1 s, 10 s and 100 s), and a time step equal to 10 s seemed to be reasonable. The influence of the mesh size on this interface was evaluated (40, 80 and 800 nodes); a grid of 80 nodes with a finer mesh near to the cold wall was found to be suitable. In order to obtain a numerical solution close to the analytical one, and taking into account a grid of 80 nodes and a time step of 10 s, it was reasonable to choose an under-relaxation coefficient ω of 0.9. The maximal relative error between numerical data and analytical values when calculating the interface position versus time is presented in Table 2.

Table 2
Maximal relative errors for the ice melting.

	Time step Δt (1–10–100 s)	Nodes (40–80–800)	Under-relaxation coefficient (0.3–0.6–0.9)
Maximal relative error (numerical/analytical) (%)	0.99	0.28	2.67

Table 3
Thermophysical properties of ice.

	Physical properties		Test conditions	
	Ice	Water		
k (W m^{-1} K^{-1})	1.92	0.606	L (m)	1 m
c_p (J kg^{-1} K^{-1})	1960	4181	T_0 (K)	268.15
ρ (kg m^{-3})	917	1000	T_F (K)	273.15
α (m^2 s^{-1})	1.07×10^{-6}	1.45×10^{-7}	T_w (K)	293.15
Ste	0.118	0251		
L_f (kJ kg^{-1})	333.4			

Table 4
Thermophysical properties of gallium.

	Physical properties		Test conditions	
	Solid	Liquid		
k (W m^{-1} K^{-1})	43.6	33	L (m)	1 m
c_p (J kg^{-1} K^{-1})	381.5	360	T_0 (K)	301.45
ρ (kg m^{-3})	5907	6093	T_F (K)	302.93
α (m^2 s^{-1})	1.9×10^{-5}	1.5×10^{-5}	T_w (K)	311.15
Ste	0.039	0.037		
L_f (kJ kg^{-1})	80.16			

Table 5
PCM test.

Test conditions	
L(m)	1 m
T_0 (K)	288.15
T_F (K)	300.15
T_w (K)	323.15

For example, the necessary time to melt a thickness of 1 m of ice was found to be about 20 days ($t = 17 \times 10^5$ s); a reasonable time, neglecting natural convection. The numerical relative error was found to be less than 0.05%.

Another test has been done for Gallium, its thermophysical properties have been placed in Table 4. This material had an initial uniform temperature $T_0 = 301.45$ K, and its temperature at $x = 0$ was raised, at $t > 0$, to $T_w = 311.15$ K. As for the previous test, its side ($x = L_x$) was maintained at T_0. The numerical predictions of the position of the interface and the temperature at the final stage of the melting ($t = 12 \times 10^4$ s) were in good agreement with the

analytical solution. The numerical relative errors were 1.06% and 0.046%, respectively.

Finally, the last test concerned the fusion and the solidification of the PCM 27 (Figs. 4 and 5). All the parameters are shown in Table 5. As for ice and gallium, the position of the interface obtained numerically are very close to the analytical one (Fig. 4). Fig. 5 of comparison concerns the solidification of PCM 27. Initially, the material was entirely liquid at temperature T_0, higher than the melting temperature T_F. At time $t > 0$, the temperature of the outer wall ($x = 0$) of the brick was brought down to a temperature $T_w < T_F$. Fig. 5 presents the position of the interface during the solidification process. The relative errors are very small, about 1.9% for the fusion, and about 1.2% for the solidification.

3.2.2. Fluent code

Continuity, momentum and energy equations were solved numerically by means of the finite volume method. The SIMPLE method within version 6.2 of the commercial code FLUENT® was utilized for solving the governing equations [33].

Simulations have been performed taking into account experimental conditions for different temperature ranges. Non-dimensional parameters of PCM 27 are summarized in Table 6.

A grid of 40×20 cells was found to be adequate to resolve the details of the flow and temperature fields with a finer grid distribution in the vertical direction. The time step for integrating the temporal derivatives was set to 0.1 s, following comparison of selected quantities obtained from simulations using 1, 0.5, 0.1, 0.05, and 0.01 s. The Power Law differencing scheme was used for solving the momentum and energy equations, whereas the PRESTO scheme was adopted for the pressure correction equation. The under-relaxation factors for the velocity components, pressure correction, thermal energy, and liquid fraction were 0.3, 0.1, 1, and 0.9, respectively. The Fluent Melting and Solidification model was used to solve the heat transfer with phase change. The driving force for the fluid motion was due to density variation under the temperature gradient, causing the natural convection phenomenon. In the Fluent code the natural convection is taken into account via the Boussinesq term. The Fluent code uses an enthalpy-porosity formulation. The liquid fraction is computed at each iteration, based on an enthalpy balance. This technique treats the mushy zone (partially solidified region in which the liquid fraction lies between 0 and 1) as a porous medium. The average velocity was about 1.7×10^{-3} m s^{-1} increasing the PCM melting.

In order to satisfy convergence criteria (10^{-6}), the number of iterations for every time step was between 200 and 400.

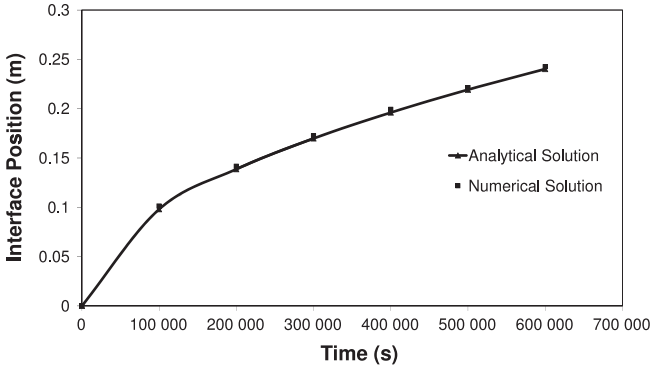

Fig. 4. Interface position of the melting of PCM 27.

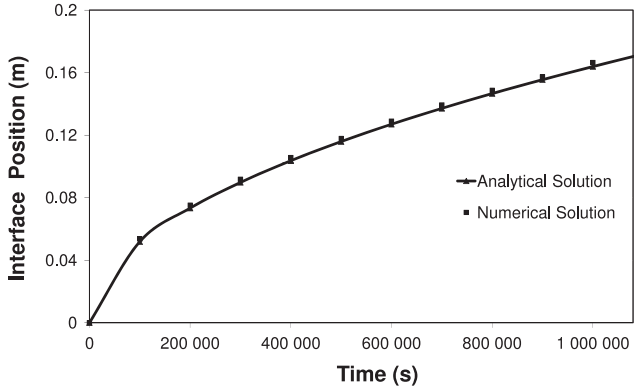

Fig. 5. Interface position of the solidification of PCM 27.

Table 6
Non-dimensional parameters of PCM 27.

R	0.12 ($L_x = 0.025$ m $- L_y = 0.21$ m)
Ra	1.34×10^8
Pr	273.85
Ste	0.2968
c_s/c_l	0.79
k_s/k_l	0.71

3.2.2.1. Boundary and initial conditions. At time $t = 0$, the PCM was taken to be a motionless solid that was maintained at a constant temperature T_0 below the melting temperature T_F of the PCM.

3.2.2.1.1. On the heated wall.

$u(x = 0, y, t) = 0$
$v(x = 0, y, t) = 0$
$T(x = 0, y, t) = T_w$

3.2.2.1.2. On the cold wall.

$T(x = L_x, y, t) = T_0$

3.2.2.1.3. On the adiabatic walls.

$$u(x, y = 0, t) = 0 \quad u(x, y = L_y, t) = 0$$
$$v(x, y = 0, t) = 0 \quad v(x, y = L_y, t) = 0$$
$$\frac{\partial T}{\partial y}(x, y = 0, t) = 0 \quad \frac{\partial T}{\partial y}(x, y = L_y, t) = 0$$

4. Results and discussion

4.1. Comparison between numerical predictions and experimental data for heat storage

The heat storage period predicted by the FDM code as well as by the Fluent® software was compared to experimental measurements. Two main parameters have a particular interest for the heat storage of a material: the time necessary for the storage (i.e. the complete fusion of PCM); and also the maximum temperature of the PCM at that instant.

Initially ($t = 0$), the material was isothermal and, at $t > 0$, was heated by modifying the temperature set point of the thermo regulated baths. The material was thus evolving from temperature T_0 to temperature T_W. Between these two permanent states the material stored energy. The fluxmeters made it possible to measure the heat fluxes exchanged at the edges of the sample. Temperatures were measured in the middle of the external and internal faces of the brick envelope to take into account a possible thermal effect produced by the material which contained the product. The experiment consisted first imposing on the sample a superficial constant temperature on the left lateral face, until a thermal steady state was obtained corresponding to an isothermal material. The heat fluxes were then zero at the initial time $t = 0$. It was also confirmed that the thermal losses were negligible at the isolated side faces.

The experiment really started at ($t_{initial}$), a sharp water temperature variation was imposed in the bath. This induced a thermal evolution of the system (storage) during the calculation time (4 h).

Temperature variations and heat flux for different cases of heat storage (latent and/or sensible) have been studied. All the data are provided from experiments, FDM 1D and Fluent code 2D. The cycles concerned the variations of the heat storage of the sample in solid phase for a temperature range from 15 °C to 20 °C and also within the liquid phase when temperature changes from 40 °C to 50 °C. Fig. 6 presents all the three different phases during the temperature range (15–50 °C). In the case of sensible storage (liquid or solid), the curves from experiments and simulations are very close (relative error of 2.2%) to each other and consequently the results are satisfactory. In the case of a phase change solid/liquid 15–50 °C (Fig. 6), the three steps of heat transfer (solid, solid/liquid, liquid) are highlighted and the period of every phase obtained from experimental data and simulation results is almost the same. However, a small difference occurs between experiments and numerical predictions in the region where both phases coexist. This result could be justified by the behaviour of the PCM 27 which is different after every solidification process, because of a random crystalline re-organization (Fig. 3).

Fig. 6 also shows that the heat stored was much more important than sensible heat transfer when a phase change occurs. This confirms the advantage of latent heat storage. A new thermal balance was reached in a little more than 3 h.

One of the advantages of the simulations was to provide data which might be difficult to obtain in an experimental device. For example, the liquid fraction versus time was easily obtained by means of the FDM code or the Fluent software. Fig. 7 shows the evolution of the liquid fraction in time predicted by both codes. The time necessary to melt the whole material calculated by simulations were almost the same as the one obtained from the experimental curve: 1.48 h by Fluent, 1.6 h by FDM and 1.68 h in the experimentation (Fig. 6). Consequently, FDM code seems to predict better fusion time than Fluent code.

4.2. Comparison between numerical predictions and experimental data for heat recovery

Solidification process is shown in Figs. 8–10 where temperature variations and heat flux are presented for different cases. In the cooling case, the temperature evolved from +20 °C to +15 °C (Fig. 8),+50 °C to +40 °C (Fig. 9) and +50 °C to +15 °C (Fig. 10).

Satisfactory results were obtained in the experimental and numerical comparison when there is no phase change (Figs. 8 and 9). However, a significant difference was observed in the phase change range. Actually, numerical simulations (Fluent and FDM codes) did not take into account the important effect of supercooling phenomenon. Generally, the average time necessary for heat recovery was very close from experimental to numerical data. The Fluent curve presents an effect unsolved and linked to the enthalpy method [34]. Stair-casing effects seem to be inherent to enthalpy methods, the interface location is determined in a post-processing step as a corresponding isotherm of the heat distribution. The use of a uniform Cartesian grid yields to a difficulty to capture the curve boundary. This effect is due to the coarseness of the grid resulted due to the trade-off between the mesh density and the solution time.

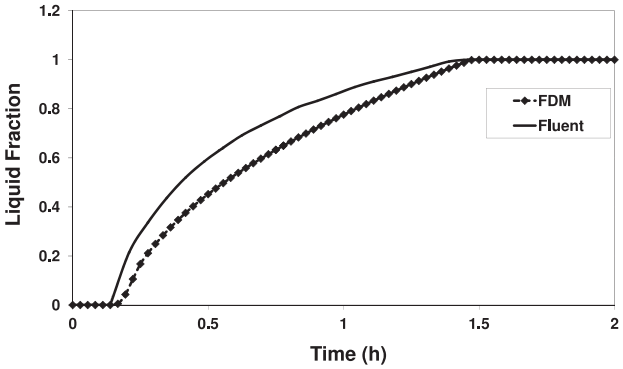

Fig. 7. Liquid fraction variation when temperature varies between 15 °C and 50 °C.

When the temperature was close to 27 °C, about 45 min after the beginning of the test, the heat flux evolution reversed. Fifteen minutes later, the surface temperature has increased from 22 °C to 26 °C, whereas the experimental heat flow has decreased. It seems that de-stored energy was reabsorbed immediately by the material (phenomenon of supercooling). From this critical moment, our sample continued to cool until +15 °C while the material was solidifying slowly. After more than five hours, it reached a new balance state.

At the beginning of solidification, a layer of solid PCM started to be formed on the plane surface in contact with the exchanging plate, a layer which "isolates" the liquid PCM. Solidification continued slowly because of low thermal conductivity of the solid PCM (k estimated in experiments at 0.45 W/m K). The temperature of the sample surface was equal to 15 °C only at the end of the test. This could be with a defect of refrigeration power of the regulated bath, which could not quickly absorb all the heat produced during the material solidification.

The results highlight the difficulties to estimate the amount and rate of heat recovery in the material due to the existence of supercooling. These difficulties pertain because of thermal conductivity differences between solid and liquid phases.

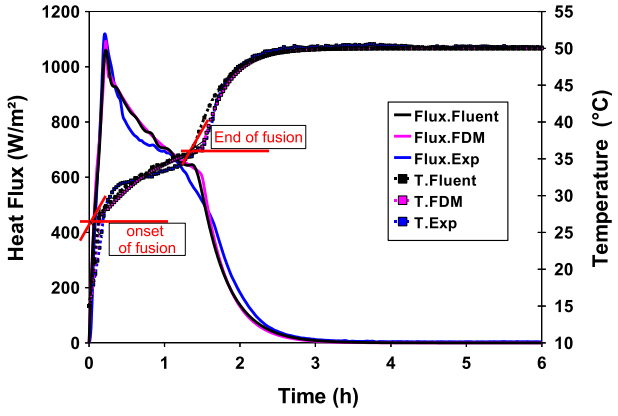

Fig. 6. Temperature and heat flux variations (15–50 °C).

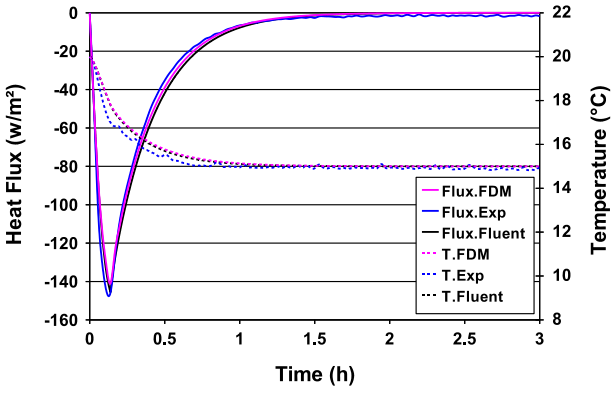

Fig. 8. Temperature and heat flux variations (20–15 °C).

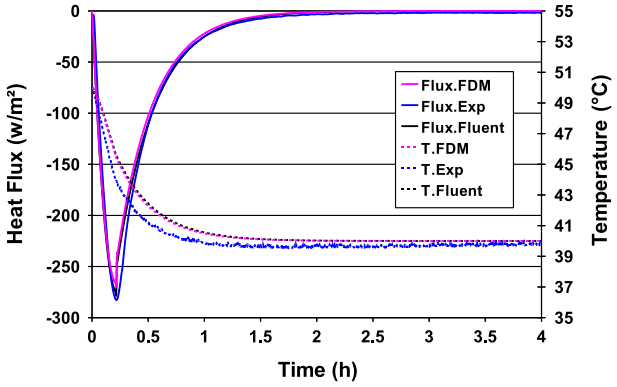

Fig. 9. Temperature and heat flux variations (50–40 °C).

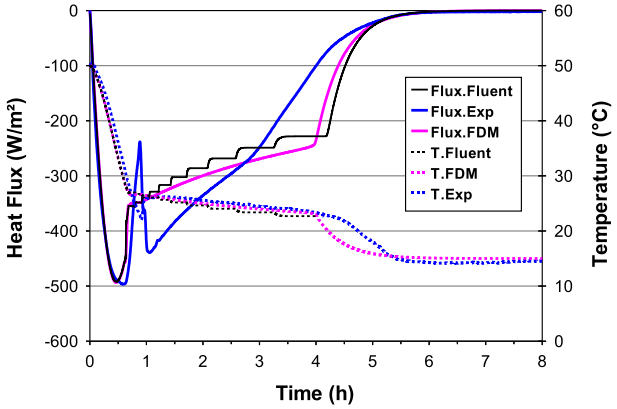

Fig. 10. Temperature and heat flux variations (50–15 °C).

Finally, in Fig. 11, the total amount of experimental heat stored (and discharged) during a complete cycle (15–50–15 °C) is presented. PCM 27 exhibits hysteresis because of the unpredictable process of crystallization [35]. The experiments were repeated and variability was observed because the onset of fusion never occurs at the same temperature. During the fusion process, the heat storage takes place at a constant temperature (about 27 °C), whereas the followed path during the solidification process is different. The temperature of the material is decreasing down to 19 °C while releasing sensible energy, corresponding at the beginning of the release of latent heat, at this stage, the first solid layer appears. Heat recovery occurs at a constant temperature about 24 °C.

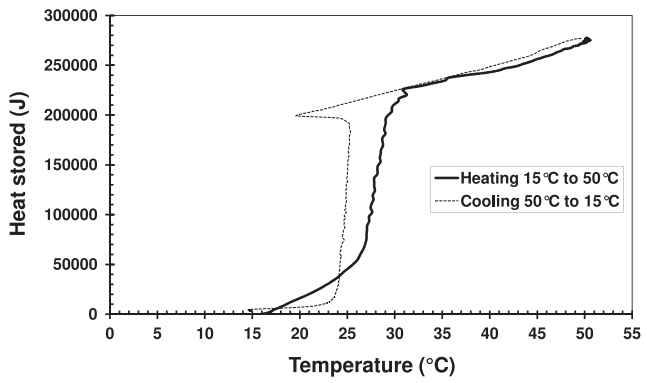

Fig. 11. Heat stored on temperature cycle (15–50 °C).

5. Conclusions

The objective of this article was to study the energy storage and the energy recovery, based on the comparison of reliable experimental data and numerical modeling, by means of the use of a phase change material. An experimental set-up was used to measure the temperatures and the heat fluxes in order to characterize the phase change effects. The influence of supercooling phenomenon has been clearly exhibited with the experimental data: the melting process started at a temperature higher than for the solidification process. No numerical simulations 1D and 2D gave satisfaction because results are very far away from the experimental ones: the codes did not represent the supercooling phenomenon. The numerical modeling showed that the supercooling phenomenon must be taken into account correctly in order to predict the PCM thermal behaviour. Further investigations are needed to have a better numerical description of this special phase change feature.

Acknowledgments

The authors are very grateful to the program ANR-PREBAT which finances the work and to Artois Comm and the Nord Pas de Calais Region.

References

[1] Cheng KC, Seki N. Freezing and melting heat transfer in engineering. New York: Hemisphere Publishing Corporation; 1991.
[2] Medrano M, Yilmaz MO, Nogues M, Martorell I, Roca Joan, Cabeza Luisa F. Experimental evaluation of commercial heat exchangers for use as PCM thermal storage systems. Appl Energy 2009;86(10):2047–55.
[3] El-Sebaii AA, Al-Ghamdi AA, Al-Hazmi FS, Faidah Adel S. Thermal performance of a single basin solar still with PCM as a storage medium. Appl Energy 2009;86(7–8):1187–95.
[4] Agyenim F, Hewitt N, Eames P, Smyth M. A review of materials, heat transfer and phase change problem formulation for latent heat energy storage systems (LHTESS). Renew Sustain Energy Rev 2010;14:615–28.
[5] Darkwa K, O'Callaghan PW, Tetlow D. Phase-change drywalls in a passive-solar building. Appl Energy 2006;83(5):425–35.
[6] Kuznik F, Virgone J. Experimental assessment of a phase change material for wall building use. Appl Energy 2009;86(10):2038–46.
[7] Xiao W, Wang X, Zhang Y. Analytical optimization of interior PCM for energy storage in a lightweight passive solar room. Appl Energy 2009;86(10):2013–8.
[8] Darkwa J. Mathematical evaluation of a buried phase change concrete cooling system for buildings. Appl Energy 2009;86(5):706–11.
[9] Martin V, He Bo, Setterwall Fredrik. Direct contact PCM-water cold storage. Appl Energy 2010;87(8):2652–9.
[10] Rady M. Thermal performance of packed bed thermal energy storage units using multiple granular phase change composites. Appl Energy 2009;86(12):2704–20.
[11] Zhou G, Yang Y, Wang X, Zhou S. Numerical analysis of effect of shape-stabilized phase change material plates in a building combined with night ventilation. Appl Energy 2009;86(1):52–9.
[12] Zalba B, Marin JM, Cabeza LF, Mehling H. Review on thermal energy storage with phase change: materials, heat transfer analysis and applications. Appl Therm Eng 2003;23:251–83.
[13] Wang WL, Yang XX, Fang YT, Ding J. Preparation and performance of form-stable polyethylene glycol/silicon dioxide composites as solid–liquid phase change materials. Appl Energy 2009;86(2): 170–4 [IGEC III – Special Issue of the Third International Green Energy Conference (IGEC-III), Vasteras, Sweden].
[14] Wang WL, Yang XX, Fang YT, Ding J, Yan JY. Preparation and thermal properties of polyethylene glycol/expanded graphite blends for energy storage. Appl Energy 2009;86(9):1479–83.
[15] Wang WL, Yang XX, Fang YT, Ding J, Yan JY. Enhanced thermal conductivity and thermal performance of form-stable composite phase change materials by using [beta]-Aluminum nitride. Appl Energy 2009;86(7-8).
[16] Cristopia, <http://www.cristopia.com>.
[17] Cordeiro Cavalcanti F. Caractérisation thermique de produits de l'état liquide à l'état, Thèse de Doctorat. Institut national des sciences appliquées de Lyon; 2006.
[18] Zeraouli Y, Ehmimed JA, Dumas JP. Modèles de transferts thermiques lors de la fusion binaire dispersée. Int J Therm Sci 2000;39:780–96.
[19] Ehmimed JA, Zeraouli Y, Dumas JP, Mimet A. Heat transfers model during the crystallization of a dispersed binary solution. Int J Therm Sci 2003;42(1):33–46.
[20] Jamil A, Kousksou T, Zeraouli Y, Gibout S, Dumas JP. Simulation of the thermal transfer during an eutectic melting of a binary solution. Thermochim Acta 2006;44(1):30–4.

[21] Yinping Z, Yi J. A simple method, the T-history method, of determining the heat of fusion, specific heat and thermal conductivity of phase change materials. Measur Sci Technol 1999;10(3):201–5.
[22] Hatakeyama T, Quinn FX. Thermal analysis. 2nd ed. Chichester: Wiley; 1999.
[23] Diaconu BM, Varga S, Oliveira AC. Experimental assessment of heat storage properties and heat transfer characteristics of a phase change material slurry for air conditioning applications. Appl Energy 2010;87(2):620–8.
[24] Younsi Z, Joulin A, Zalewski L, Lassue S, Rousse D. Thermophysical characterization of phase change materials with heat flux sensors. In Proceedings of eurotherm. The Nederlands; 2008.
[25] Leclercq D, Thery P. Apparatus for simultaneous temperature and heat flow measurement under transient conditions. Rev Sci Instrum 1983;54: 374–80.
[26] Lassue S, Guths S, Leclercq D, Duthoit B. Natural convection by heat flux measurement and anemometry using thermoelectric effects. In 3rd world conference on experimental heat transfer, fluid mech and thermod; 1993. p. 831–8.
[27] Dutil Y, Rousse DR, Ben Salah N, Lassue S, Zalewski L. A review on phase-change materials: mathematical modeling and simulations. Renew Sustain Energy Rev 2010.
[28] Voller VR. Fast implicit finite-difference method for the analysis of phase change problems. Numer Heat Trans Part B 1990;17:155–69.
[29] Costa M, Buddhi D, Oliva A. Numerical simulation of a latent heat thermal energy storage system with enhanced heat conduction. Energy Convers Manag 1997;39:319–30.
[30] Sharma A, Tyagy VV, Chen CR, Buddhi D. Review on thermal energy storage with phase change materials and applications. Renew Sustain Energy Rev 2009;13(2):318–45.
[31] Chen CR, Sharma A, Tyagi SK, Buddhi D. Numerical heat transfer studies of PCMs used in a box-type solar cooker. Renew Energy 2008;33:1121–9.
[32] Younsi Z, Joulin A, Zalewski L, Rousse DR, Lassue S. A numerical study of PCM melting heated from a vertical wall of a rectangular enclosure. Int J Comput Fluid Dynam 2009;23(7):553–66.
[33] Fluent. User's guide; 2005.
[34] Javierre E, Vuik C, Vermolen FJ, Segal A. A level set method for three dimensional vector Stefan problems: dissolution of stoichiometric particles in multi-component alloys. J. Comput Phys 2007;224:222–40.
[35] Bédécarrats JP, Dumas JP. Etude de la cristallisation de nodules contenant un matériau à changement de phase en vue du stockage par chaleur latente. Int J Heat Mass Trans 1997;40(1):149–57.